A neural circuit mechanism in medial entorhinal cortex for integrating event duration

Animals utilize interval timing—measuring time in the range of seconds to minutes—to plan and execute a wide variety of behaviors, including foraging, capturing prey, and evading threats. In this project we have focused on how medial temporal lobe structures might play a previously unrecognized role in interval timing by developing novel timing paradigms that require more flexible, context-dependent learning (**Fig. 1a,b**). We have discovered that medial entorhinal cortex (MEC), traditionally known for spatial memory, may also function as a timing system. To test this hypothesis, we developed a temporal delayed nonmatch-to-sample task (tDNMS) in which mice must learn to report whether pairs of odor stimuli are match or nonmatch in duration (Bigus et al, 2023, bioRxiv). We combined this behavioral approach with cellular resolution 2-photon Ca^{2+} imaging in MEC. Our results show that from the start of each trial, elapsed time is encoded by the regular, sequential activity of populations of MEC "time cells" (**Fig. 1c**). In separate experiments we have shown that chemogenetic inactivation of MEC is required for learning of the tDNMS task. This work underscores the critical role of the MEC in learning more complex and flexible timing behaviors. In this abstract, we propose three key questions to pinpoint the neural mechanisms in MEC that are the basis for this learning: **First, what neural dynamics of MEC time cells could support learning of timing behavior?** To address this, we have measured single cell and population Ca^{2+} dynamics of MEC 695 time cells (33.8% of active neurons;10 sessions in 6 mice) in behaving mice across learning in the tDNMS task (**Fig. 1c**). During initial training, MEC time cells tend to exhibit context-independent activity across trial types. However, over learning across days as mice's performance reaches an asymptote of ~75% correct responses, these cells shift to display context-dependent firing, selectively responding to specific trial types (**Fig. 1b**). To quantify this at the population level, we assessed the average signal correlation among MEC time cells across different trial types, finding that the Pearson's Correlation shifted 0.573 ± 0.015 on day 1 and 0.418 ± 0.017 on day N ($Z = 6.77$, $p < 0.001$, Wilcoxon rank-sum) (**Fig. 1d**). Closer examination of the time cells' sequences, sorted by peak firing within the trial, revealed reduced coherence in later phases—when sufficient information to distinguish trial types becomes available (e.g., short-short versus short-long distinguishable by an ideal observer around 7 seconds into the trial; see **Fig 1e red line**). We quantified this by creating population vectors to track moment-to-moment variations in time cell activity across trial types. Compared to a null model with randomized trial labels, actual data diverged from the null at critical trial points (**Fig. 1e**), indicating an earlier and more marked divergence through learning (divergence was defined as the time point when the real data increased above 0.1% of null distribution. For S-S vs S-L comparison: divergence shifted from 10.1 s to 9.3 s over learning. For S-S vs L-S comparison: divergence shifted from 7.2 s to 6.7 s over learning). Notably, in training sessions structured without "long-long" stimuli, "long-short" trials were identified earlier, underscoring the predictive dynamic that develops over learning in MEC time cells. Subsequent analyses with a support vector machine—cross-validated using a leave-one-out method against a surrogate dataset generated by shuffling trial identities 1,000 times—showed that most single trials could be decoded (mean accuracy across mice was 68%; $p < 0.01$ for 5 out of 6 mice; **Fig. 1f**), with accurate trial type identification occurring later in the trial as information accumulated. Together, these results demonstrate that over learning, MEC time cells transition from a context-independent to a context-dependent firing pattern, which corresponds with the animals' improved ability to discriminate trial types as sufficient information accrues within each trial.

Next, we asked what circuit mechanism in MEC drives the time-locked sequential firing of MEC time cells? Previous work suggests that the spatial firing patterns of MEC grid cells are driven by a continuous attractor network (CAN) (Burak and Fiete, 2009; Stenola et al. 2012; Yoon et al. 2013; Gardner et al. 2022). In this model, recurrent synaptic connectivity generates activity bumps localized on a 2D toroidal manifold. During navigation, the CAN integrates synaptic inputs that encode the animal's running speed and direction, generating the spatial firing patterns observed in grid cells. We hypothesized that during interval timing, MEC could be using nearly identical CAN dynamics to integrate elapsed time (Issa et al. 2020). The CAN model predicts that neurons maintain coherent relative phasic activity at all times due to local synaptic connections, even during non-task periods like the intertrial interval (ITI) or during sleep. To examine this feature of functional network connectivity, we measured the pairwise correlation structure of the population of MEC time cell activity as mice were engaged in each trial during the tDNMS task and during nontask relevant phase of the ITI. Our results demonstrate that pairs of time cells maintain their correlation during the timing task and also exhibit coherent activity during non-task relevant periods, such as the intertrial interval (**Fig. 1g**). This suggests functional connectivity, wherein cells with similar phase relationships during the task (i.e., cells that fire at comparable delay times) are likely connected

via net excitatory synaptic input, either reciprocally or through a common feedforward input. Conversely, cells with distinct phase relationships (i.e., cells that fire at different delay times) tend to exhibit reciprocal net inhibition. In our on-going work we are measuring signal and noise correlational structure over long time periods and during sleep using single unit electrophysiological methods.

Finally, we investigated which cognitive strategy animals use to solve the tDNMS time task. The tDNMS task could be solved in a number of ways and of particular interest is whether mice are timing the entire length of the trial (since non-matching trial encompass a longer total duration), timing the individual stimuli presented to search for a "go cue", or employing the more abstract strategy of timing both stimuli and then performing an explicit comparison. To address this question, we trained a regularized Poisson regression model with predictors derived from potential "cognitive strategies" that animals might be employing in order to make a decision to lick or not-lick on a given trial (**Fig. 1h,i**). The modeling approach provides an unbiased comparison between these different potential strategies for solving the tDNMS task. We then evaluate the strategies by comparing the resulting lick-probabilities to the observed behavior on held-out trials. We are able to fit each model to the animals' behavior and observe evidence that different mice may be employing distinct strategies to varying degrees. However, the model that performs best, on average, suggests that mice are generally timing both stimuli and identifying a "Go" cue rather than performing the explicit comparison step. Interestingly, mice that show evidence of attending to the timing of both cues show increased performance during the decoding of trial type (**Fig. 1j**). Finally, we are able to use the resulting lick-probabilities to draw from a non-stationary Poisson process in order to model the predicted behaviors of potential probe trials (e.g. trials with longer inter-stimuli intervals), forming the basis for future experiments which could provide further insight into which strategy mice are using.

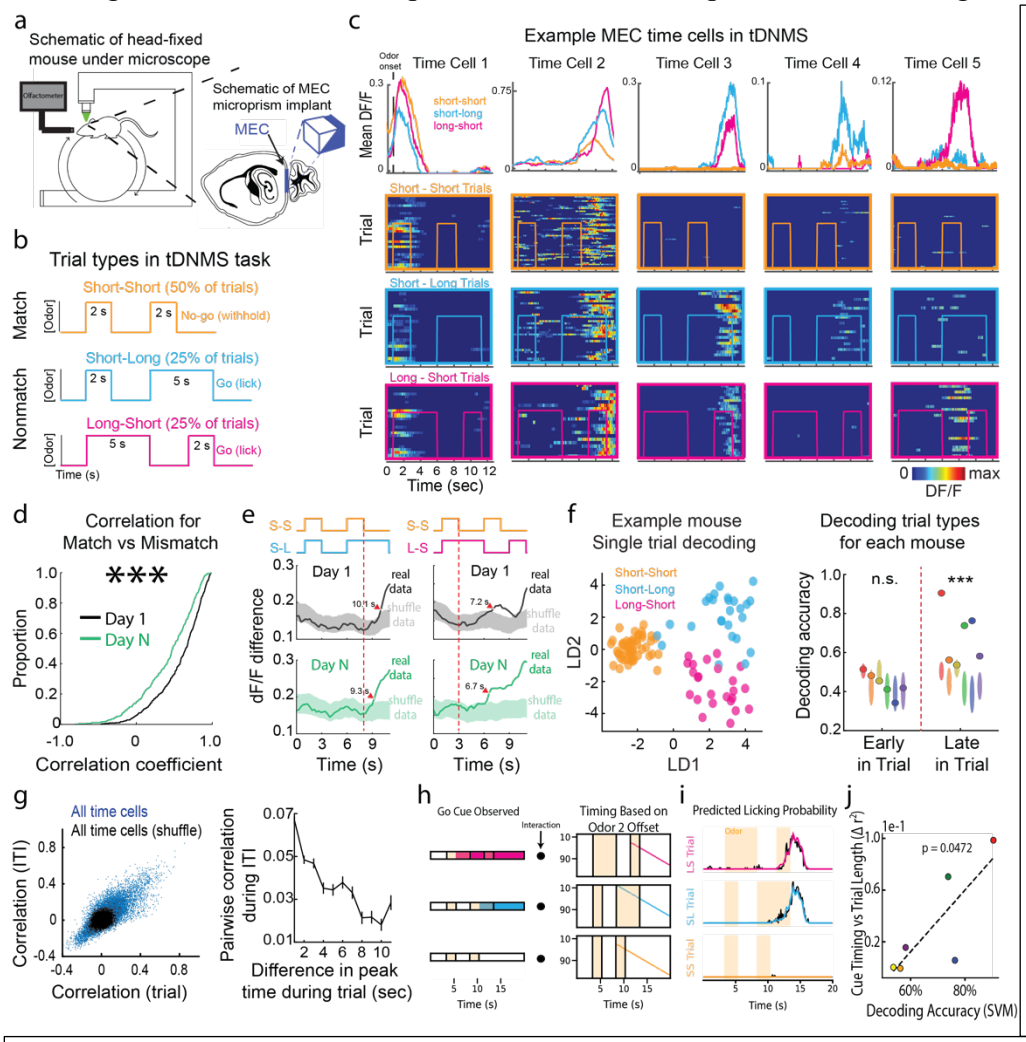

Figure 1. a. Schematic for behavioral task and 2-photon imaging method for MEC. **b.** Trial structure for tDNMS task. **c.** DF/F Ca^{2+} shown for individual MEC time cells. Time cells 1 and 2 are active across all trial types (i.e. context independent). Time cells 3-5 are active on specific trial types (i.e. context-dependent). **d.** Cumulative distribution for Pearson's correlation coefficient computed for each MEC time cell's activity across trial types for day 1 (black) and day N (green). **e.** Left, population vectors of activity difference across short-short versus short-long trial types (dark = real data; light = shuffle data). Right, same as left but for short-short versus long-short trial types. **f.** Left, LDA plots for single mouse in 1 recording session. Right, SVM decoding in early versus late in the trial for each mouse. Colored bands show noise distribution. **g**. Pairwise correlation between time cells during the tDNMS task and during the ITI for real (blue) and shuffled data (black). Right**,** Pairwise correlation of MEC time cells during the ITI as a function of their relative peak timing field activity during the tDNMS task. **h.** Predictors used for a Poisson regression model where animals time both odor cue durations. Model is based on the interaction of the animal observing the long odor as a "Go" cue and timing features anchored on the offset of the second odor. **i.** Lick probability for each trial type resulting from the model in ***h*** superimposed on mean licking (black). **j.** Animals which the modeling suggests are timing both odors show more distinct neural dynamics.